University Library

A gateway to Melbourne's research publications

Minerva Access is the Institutional Repository of The University of Melbourne

Author/s:
Reid, KJ;King, AD;Lane, TP;Short, E

Title:
The Sensitivity of Atmospheric River Identification to Integrated Water Vapor Transport Threshold, Resolution, and Regridding Method

Date:
2020-10-27

Citation:
Reid, K. J., King, A. D., Lane, T. P. & Short, E. (2020). The Sensitivity of Atmospheric River Identification to Integrated Water Vapor Transport Threshold, Resolution, and Regridding Method. JOURNAL OF GEOPHYSICAL RESEARCH-ATMOSPHERES, 125 (20), https://doi.org/10.1029/2020JD032897.

Persistent Link:
https://hdl.handle.net/11343/252714

JGR Atmospheres

RESEARCH ARTICLE
10.1029/2020JD032897

The Sensitivity of Atmospheric River Identification to Integrated Water Vapor Transport Threshold, Resolution, and Regridding Method

Kimberley J. Reid[1], **Andrew D. King**[1], **Todd P. Lane**[1], **and Ewan Short**[1]

[1]School of Earth Sciences and ARC Centre of Excellence for Climate Extremes, The University of Melbourne, Melbourne, Australia

Key Points:
- An IVT-based identification method was used to perform extensive sensitivity tests on IVT threshold and data set parameters (resolution and regridding)
- IVT thresholds below 350 kg m^{-1} s^{-1} may miss the strongest ARs when combined with a geometric criterion
- Simple methodological changes to resolution, order of operations, regridding methods, and IVT threshold can result in considerable changes to the detection results

Supporting Information:
- Supporting Information S1

Correspondence to:
K. J. Reid,
kimberleyr@student.unimelb.edu.au

Citation:
Reid, K. J., King, A. D., Lane, T. P., & Short, E. (2020). The sensitivity of atmospheric river identification to integrated water vapor transport threshold, resolution, and regridding method. *Journal of Geophysical Research: Atmospheres*, *125*, e2020JD032897. https://doi.org/10.1029/2020JD032897

Received 11 APR 2020
Accepted 12 AUG 2020
Accepted article online 7 OCT 2020

Author Contributions:
Conceptualization: Kimberley J. Reid, Andrew D. King, Todd P. Lane
Formal analysis: Kimberley J. Reid, Ewan Short
Funding acquisition: Andrew D. King, Todd P. Lane
Investigation: Kimberley J. Reid, Ewan Short
Methodology: Kimberley J. Reid, Andrew D. King, Todd P. Lane
Supervision: Andrew D. King, Todd P. Lane
Visualization: Kimberley J. Reid, Ewan Short
Writing - original draft: Kimberley J. Reid
Writing – review & editing: Kimberley J. Reid, Andrew D. King, Todd P. Lane

©2020. American Geophysical Union. All Rights Reserved.

Abstract Atmospheric rivers (ARs) are elongated narrow bands of enhanced water vapor that can cause intense rainfall and flooding. ARs only appeared in the literature the last 30 years, and there has been much debate about how to define ARs and how to identify them. As a result, a wide range of AR identification algorithms have been produced with variations in the conditions required for an object to be classified as an AR and differences in the input data. One of the key conditions in most AR identification algorithms is a minimum threshold of water vapor flux, along with geometric criteria. The aim of this study is to explore uncertainties in global AR identification based on a single integrated water vapor transport (IVT)-based identification method. We conduct a sensitivity analysis under one algorithmic framework to explore the effects of different IVT thresholds, input data resolutions, and regridding methods during the Years of Tropical Convection operational analysis (May 2008 to April 2010). We found that the resolution and regridding method affects the number of ARs identified but the seasonal cycle is maintained. AR identification is highly sensitive to the choice of IVT threshold; importantly, the commonly used 250 kg m^{-1} s^{-1} IVT threshold is not appropriate for global studies with detection methods that also include a restrictive geometric condition as this combination can lead to the strongest systems failing to be identified. The uncertainties within a single AR detection method and input data parameters may be as large as uncertainties across AR detection methodologies.

Plain Language Summary Atmospheric rivers (ARs) are large corridors of increased moisture flow in the lower atmosphere. ARs can cause hazards such as heavy rainfall, damaging winds, landslides, and flash flooding. Recently, there has been a lot of discussion about how scientists should define these weather phenomena; for example, what is the minimum amount of water needed for a weather system to be considered an AR? In order to study ARs, scientists often look at large data sets over multiple decades. So instead of searching for ARs manually in these huge data sets, they create computer algorithms that identify ARs automatically. As a result, there has been a large variety of different algorithms developed. Using a single algorithm, we answer the following question: How do small differences between data sets and moisture content of ARs affect the detection results? We found that when ARs are defined using lower thresholds of vapor transport and geometric conditions, algorithms may fail to identify the strongest ARs. Additionally, we quantified some of the uncertainty associated with using data sets of different fidelity. These results are useful for helping scientists choose the best threshold and data sets for their study.

1. Introduction

Atmospheric rivers (ARs) are elongated, conduits of water vapor that can cause extreme rainfall and flooding (Lavers et al., 2012). They are important for the global moisture budget, and studies have estimated that 90% of midlatitude (35°N) meridional vapor flux is due to ARs (Zhu et al., 1998). Newell et al. (1992) proposed the concept of "tropospheric rivers" and first used vertically integrated water vapor transport (IVT) to identify these systems. Here, IVT is defined as

$$\mathrm{IVT} = \sqrt{\left(\frac{1}{g}\sum_{1,000}^{300} qu\ \delta p\right)^2 + \left(\frac{1}{g}\sum_{1,000}^{300} qv\ \delta p\right)^2} \quad (1)$$

where g is acceleration due to gravity, q is specific humidity, u and v are the horizontal wind components in the zonal and meridional direction, respectively, and δp is the pressure difference of 100 hPa as IVT was

calculated at 100 hPa vertical increments between 1,000 and 300 hPa. Since then, a multitude of AR identification algorithms have been developed using a range of methods, thresholds, and input data, which ultimately led to the inception of the Atmospheric River Tracking Method Intercomparison Project (ARTMIP; Shields et al., 2018; Rutz et al., 2019) that aims to compare the vast number of AR identification and tracking schemes in the literature. The purpose of ARTMIP is to understand and quantify uncertainties in AR studies that may arise due to the choice of identification and tracking algorithm. This study differs and expands upon the work of ARTMIP by attempting to understand and quantify uncertainties that may arise due to the choice of data resolution, regridding method, order of operations, and IVT threshold. In our study, we keep the choice of algorithm constant to isolate the effect of other choices. There are currently 34 AR identification algorithms submitted to ARTMIP in which the three most common moisture thresholds that are used to define the boundary of ARs are: IVT $\geq$ 250 kg m^{-1} s^{-1}, (total column) integrated water vapor (IWV) $\geq$ 2 cm, and a relative threshold (usually 85th percentile of IVT or IWV).

Ralph et al. (2004) were the first to set the condition that an AR boundary could be defined by the IWV contour greater than or equal to 2 cm. This value was based on observations from the California Land-Falling Jets Experiment (CALJET) in which dropsondes were released for 2 days (25–26 January 1998) off the coast of California. Satellite measurements from a Special Sensor Microwave Imager (SSMI) were also used to calculate IWV.

The method of using a relative threshold of the 85th percentile was introduced by Lavers et al. (2012). That study used the boreal winter ARs identified by Neiman et al. (2008) and calculated the maximum IVT value along the North American west coast (e.g., the last ocean grid point) for each of 180 ARs using five reanalysis products. Then they found the median of these maximum IVT values and the percentile that corresponded with the median (values ranged from 84.4–88.3% for the five reanalyses). They determined the absolute value of IVT that corresponded with that percentile (about 500–650 kg m^{-1} s^{-1}), which became their threshold for identifying ARs. However, this relative method was based on the ARs identified by Neiman et al. (2008) who used an IWV threshold of 2 cm to identify ARs along the North American coast, in which they cite their choice of threshold being due to the Ralph et al. (2004) study. It is likely that using a relative threshold is more useful for climate change studies given the background atmospheric moisture is projected to increase with warming (Trenberth et al., 2003).

The IVT threshold of 250 kg m^{-1} s^{-1} first appears in the literature in Rutz et al. (2014). They calculated IVT using fields from the ERA-I reanalysis that had been interpolated bilinearly to 1.5° × 1.5°. Rutz et al. (2014) chose to use IVT with a threshold of 250 kg m^{-1} s^{-1} because "subjective evaluation of numerous AR events reveals that areas of IVT $\geq$ 250 kg m^{-1} s^{-1} crossing the West Coast of North America penetrate farther into the interior than coinciding areas of IWV $\geq$ 20 mm and correspond well with the spatial extent of heavy rainfall." Moreover, they tested IVT thresholds of 200 and 300 kg m^{-1} s^{-1} and concluded that while the number of identified ARs decreased with a higher threshold, the spatial pattern was about the same. Guan and Waliser (2015) and Brands et al. (2017) also included a brief threshold sensitivity analysis in their study and found little variability, although the range of thresholds used was small (85th–90th percentiles); so we have extended both of these analyses by using a much larger range of thresholds.

The most common thresholds currently used to identify ARs across the globe are derived from observations of ARs, typically in one location (western United States), or subjective evaluation of how well an IVT pattern corresponded to a precipitation pattern over a region with a relatively sparse station network. These IVT thresholds are the foundation of many recent studies on ARs including their climatology, impacts, and possible changes in a warmer world, so it is vital that we have confidence in their ability to capture AR characteristics and their robustness to the analysis of ARs across resolutions and in climate change projections. Therefore, the main aim of this study is to explore uncertainties in global AR identification based on a single IVT-based identification method. We first analyzed the effect of threshold choices on AR identification. Given that data resolution could affect the structure and magnitude of the AR representations and hence most appropriate threshold for their identification, we included changes in input data resolution and regridding method in our sensitivity study too. The study helps us to understand how small variations in the IVT field and threshold may lead to uncertainties in AR identification results.

ARTMIP aims to define and understand uncertainties in the properties of ARs solely due to identification schemes. The Tier 1 ARTMIP analysis was recently completed comparing 22 AR climatologies

(Rutz et al., 2019) using the 3-hourly Modern-Era Retrospective Analysis for Research and Applications Version 2 (Gelaro et al., 2017; MERRA v2). Rutz et al. (2019) found that different AR identification and tracking methods produced considerably different AR frequency results along Northern Hemisphere coastal transects, although they did find reasonably consistent results regarding the latitudinal location of maximum and minimum frequency along the transects. As one might expect, methods with less restrictive absolute thresholds (e.g., Gershunov et al., 2017; Rutz et al., 2014) led to higher AR frequency results along the North American and European west coasts than those with more restrictive absolute thresholds (e.g., Connect500 and Connect700 by Sellars et al., 2013). However, even among methods that use similar IVT thresholds (e.g., Tempest with absolute IVT > 250 kg m^{-1} s^{-1} and a relative threshold based on the local Laplacian of IVT and Rutz with absolute IVT > 250 kg m^{-1} s^{-1}) there were considerable differences in AR frequency, which suggests more work is needed to understand AR identification method sensitivity.

Furthermore, Hagos et al. (2015) and Swenson et al. (2018) conducted modeling studies to determine how model resolution affects AR detection results. These two studies came to opposing conclusions where Hagos et al. (2015) found that AR frequency decreased as resolution increased and Swenson et al. (2018) showed that AR frequency decreased as resolution decreased. Therefore, we have included an analysis of AR detection sensitivity to the resolution of the input IVT field. For our analysis we used high-resolution data from the Years of Tropical Convection (YoTC; Waliser et al., 2012) operational analysis archive and systematically downgraded the resolution of those data to assess the resolution sensitivity of AR identification (details can be found in section 2.4).

The remainder of this paper is organized as follows. In section 2, we explain the data sets, regridding methods, and AR identification scheme used throughout this study. Section 3 presents results from the sensitivity analysis of resolution and regridding, followed by an analysis of threshold sensitivity. Finally, in section 4, we will summarize and discuss some of the implications of these results.

2. Data and Methods

2.1. Data

We calculated daily (00UTC) IVT using Equation 1 and horizontal wind and specific humidity fields from the European Centre for Medium-Range Weather Forecasts' (ECMWF) YoTC operational analysis at the native resolution (0.125° × 0.125°; Waliser et al., 2012). The YoTC data set begins in May 2008 and ends in April 2010, and we used the entire 2 year period throughout this study. Despite being limited to 2 years, the YoTC time period includes several significant AR events (e.g., the AR that resulted in record-breaking rainfall and flooding in parts of the United Kingdom on 19 November 2009; Lavers et al., 2011). While 2 years is not long enough to examine climate mode influences, the 2008–2010 window includes both El Niño and La Niña periods, which likely makes it more representative than a period with only El Niño or La Niña. In addition, early results from ARTMIP have indicated that the choice of detection scheme has a greater influence on AR variability than the choice of reanalysis (Ralph et al., 2019). For these reasons, we concluded the YoTC data set covers an appropriate time period for quantitative analysis of AR sensitivity testing.

Additionally, we used the 40 year (1979–2018) record of IVT from ECMWF's ERA5 reanalysis at the native resolution (0.25° × 0.25°; Hersbach et al., 2019) to further validate some of our results.

2.2. AR Identification Scheme

The aim of this study was to assess the resolution, regridding, and threshold dependence of AR detection; therefore, we used a single identification scheme that was representative of the schemes commonly used in the literature. First, the scheme applies a threshold to the input IVT field to extract regions of IVT above the specified threshold. The threshold values tested were: 150, 250, 350, 500, 750 or 1,000 kg m^{-1} s^{-1}, however for the experiments that tested the sensitivity of the resolution or regridding method, we kept the IVT threshold constant at 250 kg m^{-1} s^{-1}. This value was chosen because of its prevalence throughout the literature. Next, we used ellipse fitting to find AR parameters and stored the centroid location (of the fitted ellipse), mean IVT over the ellipse, maximum IVT, major axis length, minor axis length, and orientation. The method fits an ellipse to each of the regions extracted via thresholding and ensures the ellipse has the same normalized central moments as the thresholded region. Mathematically, the major and minor axes are the eigenvectors of the covariance matrix associated with the extracted regions of IVT, and the centroid

is the center of mass of the IVT field. The length in pixels was converted to kilometers using the equation for arc length on a sphere. These potential ARs and their associated parameters were then tested against the following geometric conditions, and if all conditions were met, the potential ARs were deemed actual ARs.

The required geometric conditions were the following:

1. AR major axis length must exceed 2,000 km (e.g., Neiman et al., 2008; Rutz et al., 2014)
2. The length-to-width ratio must exceed 2 (e.g., Guan & Waliser, 2015; Pan & Lu, 2019; Shields & Kiehl, 2016; Viale et al., 2018; Wick et al., 2013)
3. The orientation angle must exceed 10° relative to lines of latitude. The purpose of this criterion is to exclude persistent zonally oriented structures (e.g., the intertropical convergence zone and Australian monsoon), which may otherwise meet the criteria for ARs.

Figure 1 illustrates what this identification scheme "sees" as ARs. Figure 1a is the global IVT field from YoTC for 19 November 2009. Note the strong AR over the North Atlantic Ocean, which led to heavy flooding in the United Kingdom (Lavers et al., 2011). Figure 1b shows the regions that are considered to be part of an AR when setting the IVT threshold of the identification scheme to 250 kg m^{-1} s^{-1}, and Figure 1c shows the same as Figure 1b but with an IVT threshold of 500 kg m^{-1} s^{-1}. We are confident our identification scheme adequately captures ARs with some exceptions such as particularly zonal ARs like that over the North East Pacific in Figure 1a.

2.3. Comparison to Other Identification Schemes

We tested how representative our identification scheme was of other methods by recreating Figure 2 from Rutz et al. (2019), in which they show an example of an AR over the West Coast of the USA at 0000 UTC on 15 February 2014 and plot the outline of what 19 of the ARTMIP methods identify as an AR. Instead, in our Figure 2 we show the number of ARTMIP algorithms that identify an AR at a given grid space, using the binary AR fields available via the ARTMIP Tier 1 catalog, and show the outline (red line) of what our algorithm identifies (using an IVT threshold of 250 kg m^{-1} s^{-1}) as an AR for that case using the same data set (MERRA v2). We found that our algorithm performs similarly to the majority of the ARTMIP methods. This gives us confidence that sensitivity analysis results based on our algorithm may help the community understand why some AR methods perform differently from others. Additionally, while we only test the sensitivity using one algorithm, the fact that our method uses similar thresholds and geometric requirements as other identification methods, and is comparable to other ARTMIP algorithms, should motivate future studies to consider these sensitivities we have found.

2.4. Resolution Degradation Methods

We degraded the resolution of the YoTC IVT fields by taking the area-weighted average of the higher-resolution horizontal winds and specific humidity fields (0.125° × 0.125°) and regridding the result onto coarser grids (0.25° × 0.25°, 0.75° × 0.75°, and 1.5° × 1.5°), using the xarray package in Python (Hoyer & Hamman, 2017), and then calculating the IVT at the new resolution to compare how different resolutions of input data affect AR identification. The purpose of simple averaging removes the smallest resolvable scales—an approach that best mimics what might be expected from coarser model resolutions (e.g., CMIP5-type climate models). Additionally, we regridded the native YoTC resolution data to 1.5° × 1.5° using two different interpolation methods to determine whether the method in which the input data were regridded affects AR identification. We used Climate Data Operators to perform bilinear and first-order conservative interpolations (Schulzweida, 2019). When comparing individual ARs, they were considered the "same" if they occurred within ±5° latitude and longitude on the same day.

3. Results

This study showed considerable variability in the temporal and spatial distributions of ARs over the YoTC time period for different thresholds, resolutions, and regridding methods. Figure 3 shows the global monthly count of ARs over the YoTC period. As the resolution of the IVT field is degraded from 0.125° to 1.5°, the magnitude of ARs decreases; however, the seasonal cycle is maintained (Figure 3a). The bilinear interpolation method led to fewer ARs being identified than the conservative method or averaging, but again the seasonal cycle is consistent with the native resolution (Figure 3b). This result may have implications for studies

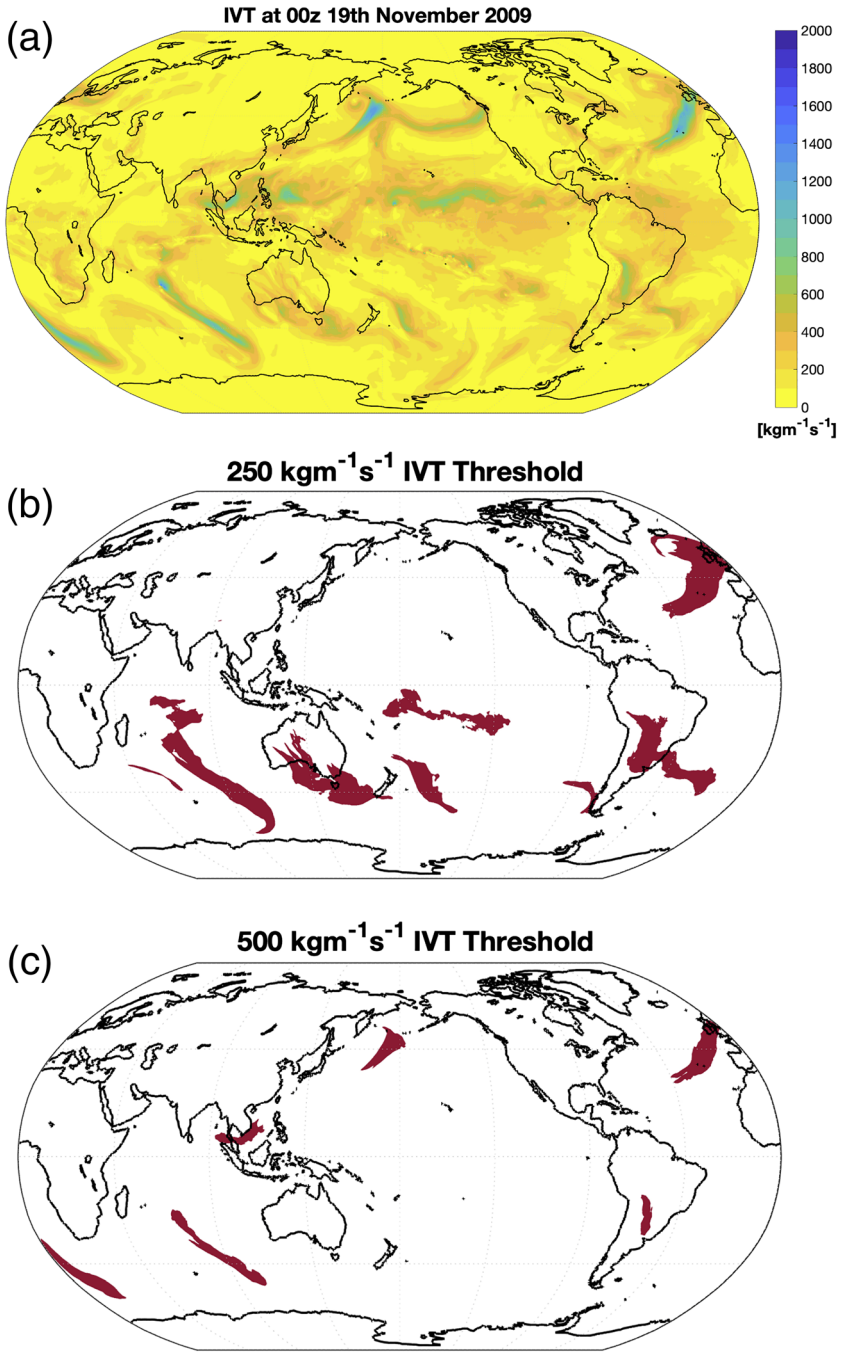

Figure 1. (a) Global IVT field at 00 UTC on 19 November 2009 calculated from YoTC *u*, *v*, and *q*; (b) mask of ARs identified by our algorithm with an IVT threshold of 250 kg m^{-1} s^{-1}; and (c) same as (b) but for a threshold of 500 kg m^{-1} s^{-1}.

of ARs that used a nonnative ERA-Interim grid prior to 2016. The ECMWF operational interpolation software used a bilinear interpolation to coarsen ERA-Interim fields (Maciel et al., 2017). The conservative regridding method appears to reproduce a seasonal cycle that is most similar to the results from the native grid; however, the conservative method also tended to produce longer ARs (600 km longer on average; Figure S1 of AR length distribution in supporting information). Regridding by averaging led to ARs that were geometrically consistent with the native resolution. The median length (~3,750 km) we found using the native and averaged grids was also consistent with the results of

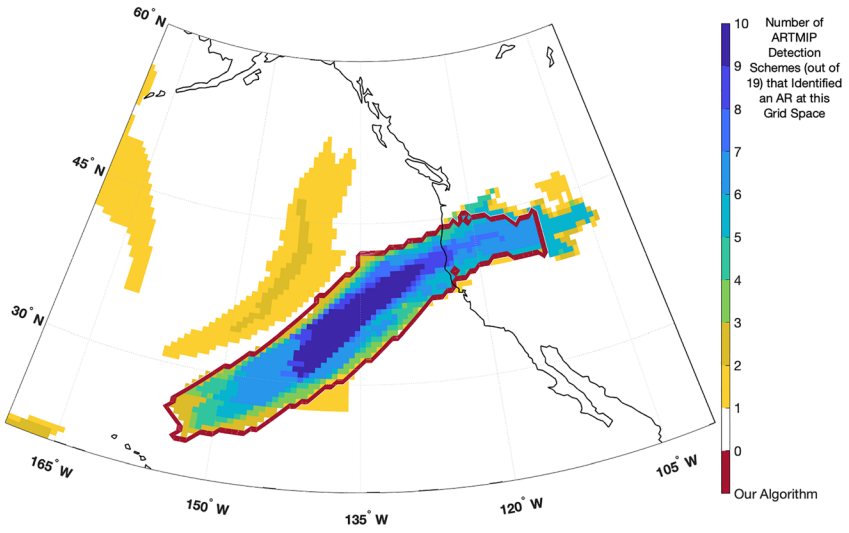

Figure 2. Density of number of algorithms identifying an AR at each grid space on 0000 UTC on 15 February 2014 (as in Figure 2 of Rutz et al., 2019) and outline (red) of the region identified as an AR using our algorithm at the same time step and same data set (MERRA v2). We used the same ARTMIP methods as in Figure 2 of Rutz et al., 2019 except we used Pan_Lu in place of Guan_Waliser.

Guan and Waliser (2015) who produced a climatology of global AR characteristics based on 18 years of data. Our results give us confidence that using coarser resolution data sets (up to 1.5° latitude-longitude) leads to AR identification with our method that is consistent with higher-resolution data in regards to seasonality and median geometric features, although coarse resolution data will likely lead to a reduced AR count. However, modeling studies of ARs such as Hagos et al. (2015) found the opposite relationship between resolution and AR counts indicating that there remains significant uncertainty in the relationship between model uncertainty and ARs. Some aspects of this sensitivity are likely related to the specific detection method but also to how well the physical aspects of the ARs are actually being resolved (which would likely also be case dependent).

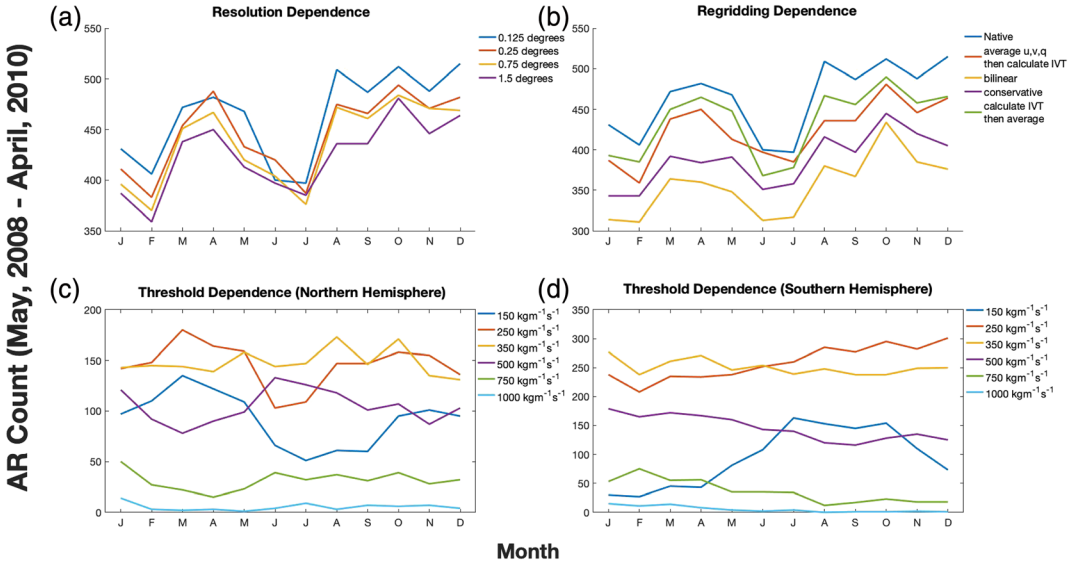

Figure 3. Global AR count for each month over YoTC period. Lines indicate different (a) IVT input resolutions, (b) regridding methods of IVT field from native to coarse resolution (1.5° × 1.5°), and identification scheme thresholds in the (c) Northern Hemisphere and (d) Southern Hemisphere. A threshold of 250 kg m^{-1} s^{-1} was used for (a) and (b).

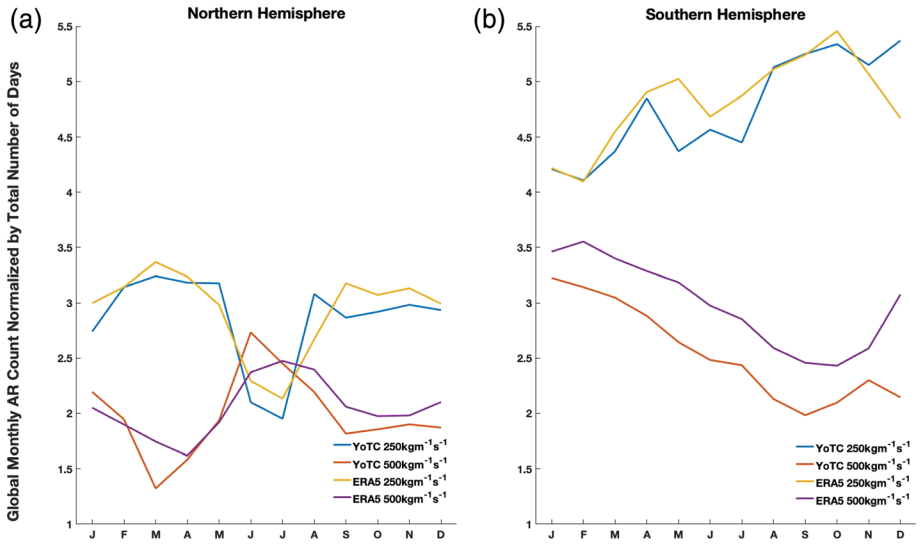

Figure 4. Normalized frequency of AR counts per month in the (a) Northern and (b) Southern Hemispheres using YoTC and ERA5 IVT fields at their native resolutions (0.125° and 0.25°, respectively) at 250 and 500 kg m^{-1} s^{-1} thresholds. AR counts were normalized by number of days in the time period used, which was 1979–2018 for ERA5 and the entire YoTC period (May 2008 to April 2010).

AR identification scheme outputs seem to be most sensitive to the threshold applied to the IVT field (Rutz et al., 2019). Rutz et al. (2014) tested the difference between an IVT threshold of 200 and 300 kg m^{-1} s^{-1} and found that while the number of ARs decreased with a higher threshold, the spatial distribution was similar for the West Coast of the United States. Rutz et al. (2019) also found methods with varying thresholds led to different AR counts along transects of western European and western North America. Our results suggest that on a global scale, threshold affects both magnitude and pattern of the AR distribution. Figures 3c and 3d show the seasonal distribution of AR count for each threshold and hemisphere. We concluded that the 150 kg m^{-1} s^{-1} threshold is too low to be useful as it includes the majority of the Earth's surface on any day. What is striking about Figure 3c (and to a lesser extent Figure 3d) is that the seasonal cycle that appears at the 250 kg m^{-1} s^{-1} threshold is not apparent at the higher thresholds. The Northern Hemisphere 250 kg m^{-1} s^{-1} threshold seasonal cycle broadly follows the seasonality that was found in Rutz et al. (2019), who looked at the month of maximum AR frequency along several Northern Hemisphere transects for different ARTMIP methods and found the maximum AR frequency typically occurred in boreal autumn to winter, while boreal summer rarely had the maximum AR frequency for most methods, although Rutz et al. (2019) also showed regional difference in seasonality.

The Northern Hemisphere has a slightly stronger seasonal cycle than the Southern Hemisphere, which we suspect is due to the relative ocean and land areas in each hemisphere affecting the seasonal cycle in meridional temperature gradients and therefore seasonal cycle in fronts and cyclones, which are typically associated with ARs. To test whether this result may be due to the YoTC data set or specific 2 year period, we repeated this analysis using ERA5 IVT from 1979–2018 for thresholds 250 and 500 kg m^{-1} s^{-1}(Figure 4). We found that for the 40 years of ERA5 data, the monthly mean AR count identified using the more restrictive threshold is also higher than the count for the less restrictive threshold during some months. Moreover, when normalized to account for difference in time period, ERA5 and YoTC IVT fields lead to similar AR counts and seasonal cycles. Furthermore, in both hemispheres, the seasonal cycle appears to be reversed for the two thresholds.

Our analysis suggests that the order in which the IVT field is calculated and coarsened impacts the final AR count. Figure 5 shows the global AR count over the YoTC period (May 2008 to April 2010) for each threshold when the horizontal wind and specific humidity fields are coarsened before the IVT is calculated (left) and when the IVT is calculated first at the native resolution then coarsened to 0.25° (right). We found differences in the number of ARs identified for some months using the two methods (Figure 5), and these differences in

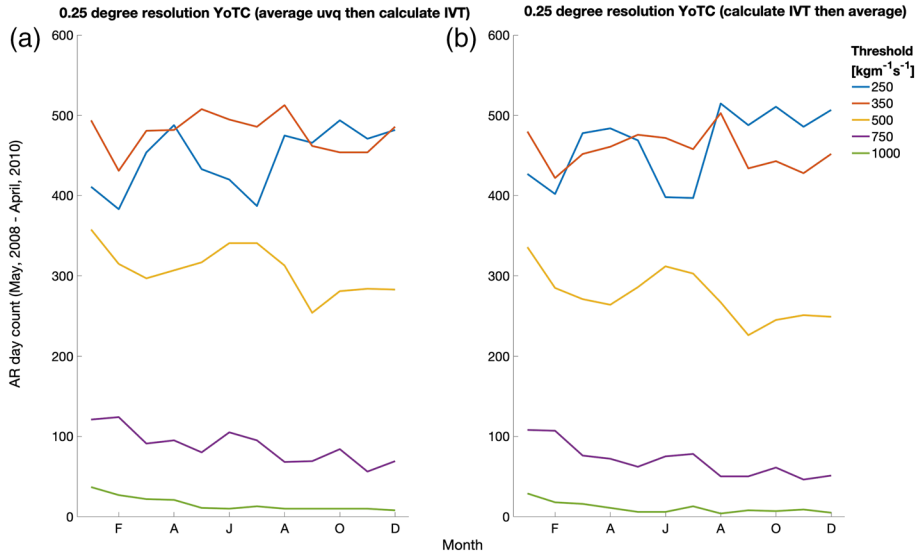

Figure 5. Global AR count for each month over YoTC period using an IVT field coarsened to 0.25°. (a) u, v, and q were coarsened, then IVT was calculated, and (b) IVT was calculated first at the native resolution then the IVT field was coarsened.

the annual cycle are most prominent at lower thresholds. Using the former method, where u, v, and q are averaged before IVT is calculated, and the method most akin to model parameterization, since models parameterize the variables of the dynamical core (e.g., u, v, and q) rather than derived values (e.g., IVT), the 350 kg m^{-1} s^{-1} threshold identifies more than the 250 kg m^{-1} s^{-1} threshold in almost every month. This result may have implications for studies using the new ERA5 reanalysis because (unlike ERA-Interim) IVT is an output variable. Therefore, if users are coarsening the data (e.g., for model evaluation) they may find a difference in AR counts if they coarsen the output IVT from ERA5 or if they coarsen the horizontal wind and specific humidity fields and then calculate the IVT themselves. However, using a higher IVT threshold (e.g., 500 kg m^{-1} s^{-1}) appears to reduce this sensitivity.

In addition to the number of ARs, we compared the spatial variability in AR occurrence at different thresholds. Figure 6 shows the proportional difference in the number of ARs identified between lower and higher thresholds. The AR location is defined by the centroid of the ellipse that was fitted during the identification process described in section 2.2. While generally we expect lower thresholds to identify more ARs than higher thresholds, Figure 6 shows regions where the lower thresholds are leading to fewer ARs being identified especially in the Pacific Ocean. We also found the distribution of AR centroid latitudes (supporting information Figure S2) was statistically significantly different ($p < 0.05$ using the Kolmogorov-Smirnov test) between all thresholds except the 750 and 1,000 kg m^{-1} s^{-1} thresholds. This suggests that more restrictive thresholds identify ARs that may not simply be a subset of those identified via less restrictive methods as Rutz et al. (2019) alludes to with the exception of the 1,000 kg m^{-1} s^{-1} threshold ARs possibly being a subset of the 750 kg m^{-1} s^{-1} detected rivers (these distributions are shown in supporting information Figure S2). Also, there is a regional signature to this effect with locations in the Pacific Ocean where the hypothesis that ARs identified by higher thresholds are a subset of those identified from lower thresholds break down.

Again, we repeated this analysis with the 40 year ERA5 data (Figure 7a) to assess the difference between AR counts using the 250 and 500 kg m^{-1} s^{-1} thresholds. We found a similar result to what we found using the 2 year YoTC data. In some regions the more restrictive thresholds led to more ARs being identified than the less restrictive threshold especially in the highly studied North Pacific Ocean. Figure 7b shows the AR centroid difference between the 2 year YoTC and 40 year ERA5 (both normalized by the number of days in each time period and ARs identified using a 250 kg m^{-1} s^{-1} threshold). We found noisy and small magnitude differences, which gives us confidence that the differences in Figure 7b are likely random and may be time period dependent (i.e., the shorter YoTC time period will have more variability than the longer ERA5 time period), and therefore the results identified using Figure 6 are unlikely to be due to the choice of data set.

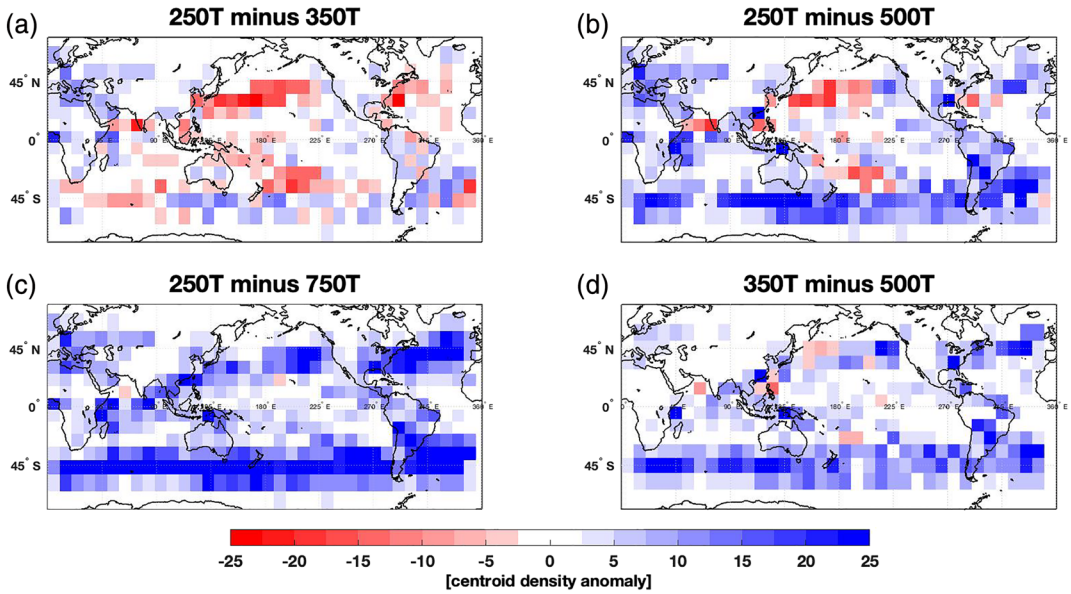

Figure 6. Difference in centroid density calculated from YoTC data between IVT thresholds of (a) 250 and 350, (b) 250 and 500, (c) 250 and 750, and (d) 350 and 500 kg m^{-1} s^{-1}.

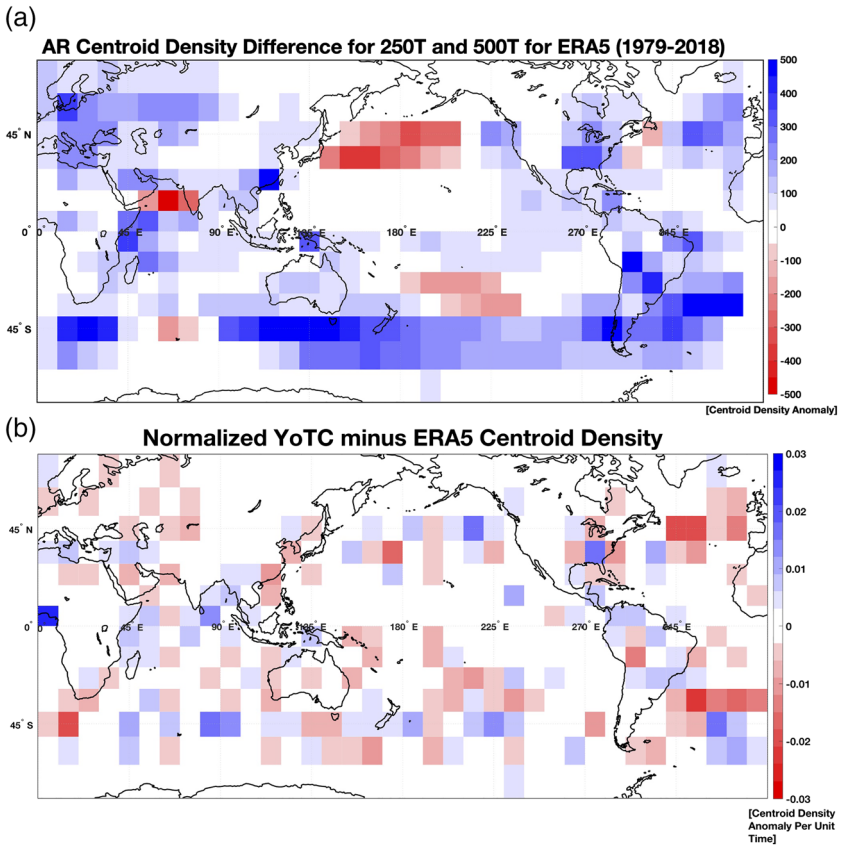

Figure 7. (a) Same as Figure 6b except for 40 years of ERA5 data and (b) difference between normalized YoTC 2 year and normalized ERA5 40 year centroid density (both at 250 kg m^{-1} s^{-1} threshold).

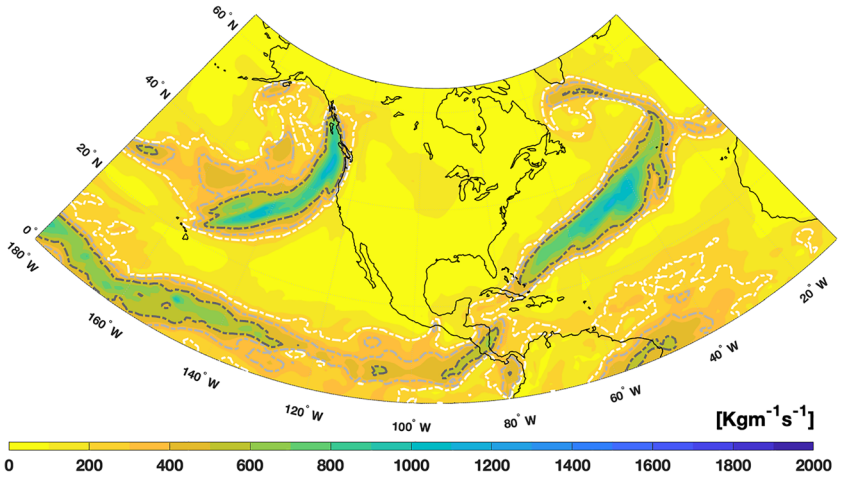

Figure 8. Example of two ARs (one in the North Pacific and one in the North Atlantic) on 11 January 2010, a day with the maximum difference in global AR count between the 500 and 250 thresholds (500 identified more). Dashed contours show 250 (white), 350 (light gray), and 500 (dark gray) IVT. Of the two ARs in this example, neither were identified by the 250-threshold scheme, and both were identified by the 350 and 500 schemes using YoTC data.

Given the unexpected result of the lower threshold of 250 kg m^{-1} s^{-1} leading to fewer ARs being identified than the 350 and 500 kg m^{-1} s^{-1} thresholds in some months, we analyzed this further by selecting a case study. We chose the day when the algorithm produced the greatest deficit in global AR count (a difference of 5 ARs on 11 January 2010) at the 250 kg m^{-1} s^{-1} threshold compared to the 500 kg m^{-1} s^{-1} threshold and plotted the IVT field (Figure 8). We found the 250 kg m^{-1} s^{-1} threshold did not identify either of the ARs in the North Pacific and North Atlantic in Figure 8, but the 350 and the 500 kg m^{-1} s^{-1} thresholds identified both ARs.

If we examine the location of the threshold boundaries (dashed lines Figure 8), we can see the 250 kg m^{-1} s^{-1} (and to a lesser extent the 350 kg m^{-1} s^{-1}) thresholds encompass much broader regions than the 500 kg m^{-1} s^{-1} threshold. We show this for two additional cases in the supporting information. We hypothesized that use of the lower IVT threshold results in the geometry conditions of the identification scheme, specifically the requirement for the length-to-width ratio to exceed 2, to fail; hence, the algorithm does not identify an AR. We tested this hypothesis by rerunning the AR identification scheme with a reduced length-to-width ratio criterion then separated the ARs that were identified exclusively with the lower ratio from those identified by the higher ratio. We then calculated the fractional difference in AR count with reduced length-to-width ratios in each basin and for three IVT thresholds (Table 1). Our results show that as the IVT threshold increases, the sensitivity of AR count to length-to-width ratio decreases. Moreover, at the lower IVT threshold, the North Pacific and North Atlantic basins have the largest fractional difference in AR count with the lower length-to-width ratio, which is consistent with Figures 6 and 7 where most of the difference in centroid density occurs in those basins along with the South Pacific. It follows, somewhat counterintuitively, that using thresholds that are too low (including the commonly used 250 kg m^{-1} s^{-1} threshold) leads to AR identification schemes failing to identify the most intense ARs. This point is

Table 1
Fractional Difference in Number of ARs Identified in Each Basin for IVT Thresholds of 250, 350, and 500 kg m^{-1} s^{-1} When the Length-to-Width Ratio Criterion is Relaxed (Reference: $L/W \geq 2$).

	$L/W \geq 1.5$			$L/W \geq 1.1$		
	250 kg m^{-1} s^{-1}	350 kg m^{-1} s^{-1}	500 kg m^{-1} s^{-1}	250 kg m^{-1} s^{-1}	350 kg m^{-1} s^{-1}	500 kg m^{-1} s^{-1}
North Atlantic	0.16	0.10	0.04	0.24	0.14	0.05
South Atlantic	0.13	0.07	0.03	0.19	0.09	0.03
Eurasia	0.09	0.06	0.16	0.12	0.070	0.20
South Indian	0.09	0.05	0.02	0.13	0.07	0.03
North Pacific	0.17	0.10	0.04	0.25	0.14	0.06
South Pacific	0.14	0.08	0.05	0.20	0.11	0.06

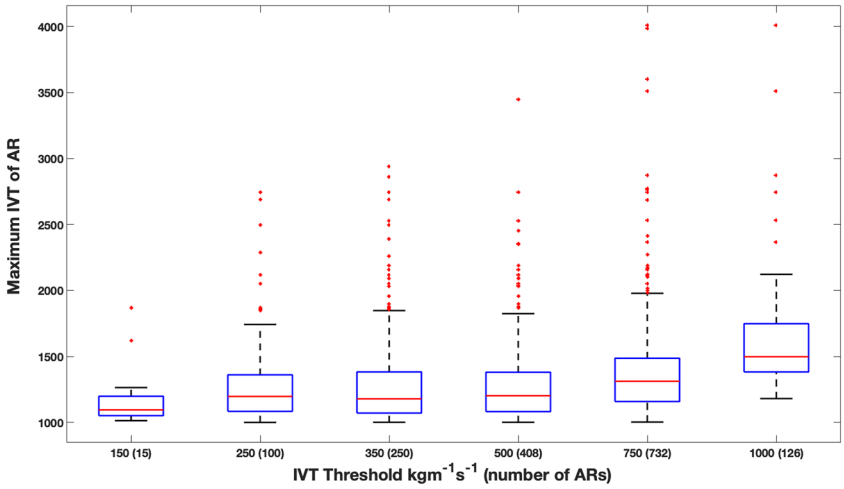

Figure 9. Box and whisker plots of maximum IVT of each atmospheric river identified using the six IVT thresholds and YoTC data set. For fair comparison, all values below 1,000 kg m^{-1} s^{-1} were excluded. Red line is the median, blue box is the interquartile range (IQR), whiskers are the most extreme points not considered outliers, and red dots are outliers defined where the difference from the median is greater than 1.5 times the IQR.

illustrated quantitatively in Figure 9, which shows boxplots of maximum IVT of each AR identified using each of the IVT thresholds. Despite identifying more ARs overall, the algorithms with the lower thresholds identified fewer intense ARs.

Given the Rutz et al. (2014) study, that defined the IVT threshold of 250 kg m^{-1} s^{-1}, was based on ERA-Interim data at a resolution of 1.5° × 1.5°, we wanted to test the hypothesis that the choice of threshold may depend on the resolution. For example, 250 kg m^{-1} s^{-1} may be appropriate for an IVT field resolution of 1.5° × 1.5° as in Rutz et al. (2014), but a higher threshold may be needed for finer-resolution IVT fields. This is an issue of relevance for optimizing AR detection in numerical weather prediction and seasonal prediction models as well as for future higher-resolution climate models. We tested the resolution effect on optimizing threshold selection by assessing whether the ARs identified using the native resolution at each threshold are the same as the ARs identified using coarser resolutions at different thresholds. The number of "same" ARs was normalized by the number of ARs identified using the native resolution field for each threshold. Hence, a value of 1 (Figure 10) indicates that the AR identification scheme finds identical ARs from the two different IVT fields, and a value of 0 indicates that the two IVT fields produce completely different ARs. Our results (Figure 10) indicate that the choice of threshold does not need to vary with resolution. Moreover, sensitivity to resolution decreases as the threshold increases. This is evident by the similarity scores between the output from the AR identification schemes with varying data resolution and threshold. Comparing the ARs identified using the native resolution of YoTC and 250 kg m^{-1} s^{-1} IVT threshold and ARs identified with a 0.25° resolution IVT fields and 250 kg m^{-1} s^{-1} IVT threshold, we calculated a value of 0.66 (Figure 10, Row 1, Column 1 [top left]). This indicates that ~34% of the ARs identified with different resolutions but the same 250 kg m^{-1} s^{-1} IVT threshold were distinct, whereas, for example, the same comparison with an IVT threshold of 500 kg m^{-1} s^{-1}produced a similarity score of 0.86 (Figure 10, Row 3, Column 3 [i.e., third from top, center column]). In addition, in each column, the combinations of thresholds and resolutions that had identical thresholds consistently showed higher values with the exception of the final column, which had the smallest sample size and is therefore quite noisy.

To further show the relationship between resolution and detection uncertainty, we undertook an idealized mathematical investigation. Figure 11 illustrates IVT threshold sensitivities to both the size of the AR and the resolution of data sets we use for their identification. First, we approximate the AR cross section as a Gaussian curve with width parameter w and cross-sectional length, y, or width, x, (i.e., along the semimajor or semiminor axes):

$$\mathrm{IVT}(y, w) = \mathrm{IVT}_0 e^{\left(-\frac{y^2}{w^2}\right)}$$

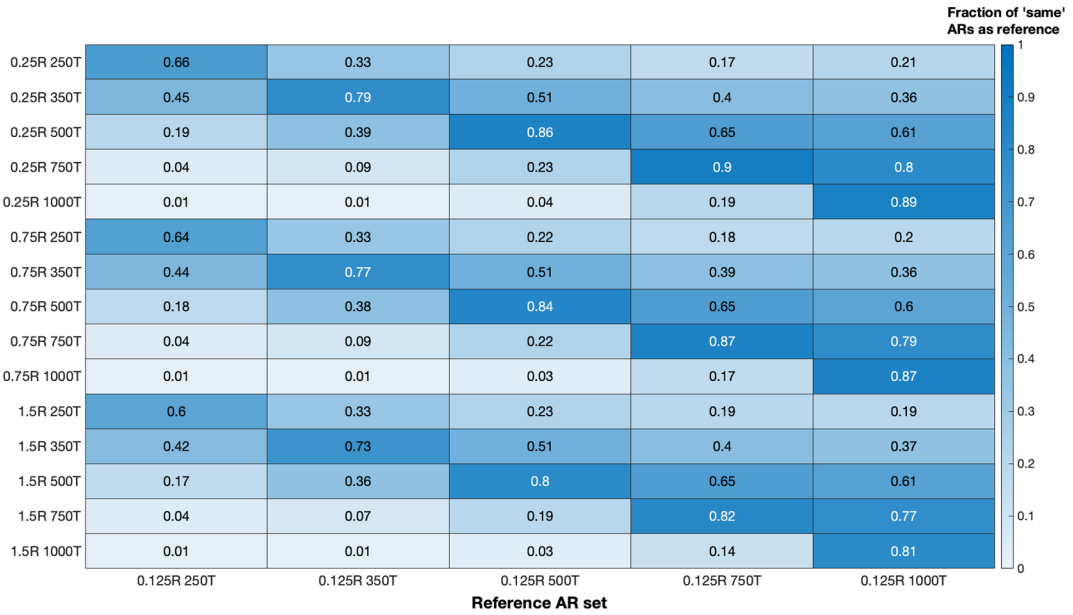

Figure 10. Heatmap showing the fraction of "same" (centroid within ±5° latitude and longitude on the same day) ARs identified using different resolutions (*value*R is resolution in °) of YoTC and IVT thresholds (*value*T is IVT threshold in kg m^{-1} s^{-1}) relative to the native YoTC resolution at each threshold. A value of 1 indicates that the AR identification scheme finds identical ARs from the two different IVT fields, and a value of 0 indicates that the two IVT fields produce completely different ARs.

We want to understand to what extent "gridding" this idealized IVT function introduces errors, which may affect sensitivity to identification thresholds (see Figure 11a for schematic). Consider a grid size of s km. Then the "gridded" or average IVT for a grid cell centered at the point y is

$$\overline{\mathrm{IVT(y,\ s,\ w)}} = \frac{1}{\mathrm{s}}\int_{\mathrm{y}-\frac{\mathrm{s}}{2}}^{\mathrm{y}+\frac{\mathrm{s}}{2}} \mathrm{IVT_0 e}^{\left(-\frac{y'^2}{w^2}\right)}\mathrm{dy'}$$

We can then compare $\overline{\mathrm{IVT}(y,\ s,\ w)}$ with the value of IVT(y, w) or more appropriately with IVT($y \pm s/2$) as, for an increasing or decreasing function, errors between function and average are largest at end points. By performing this comparison at multiple points y, and for multiple choices of s and w, we can assess sensitivity to AR size and grid size. We expect error to go to 0 as $s \to 0$ and $w \to \infty$. We chose an arbitrary value of 800 kg m^{-1} s^{-1} for IVT_0.

Figures 11b–11e indicate that the errors associated with grid size are largest for coarser grid spaces and smaller spread parameters. The errors also exhibit a nonlinear relationship with grid spacing. Given that smaller spread parameters lead to a larger error in IVT, it follows that a coarser grid space leads to greater errors along the minor axis of an AR than the major axis. Since the errors are positive, this would imply that coarsening the grid space leads to "wider" ARs. This may explain why we see fewer ARs identified with coarser grids for an algorithm with a geometric requirement such as a minimum aspect ratio.

4. Summary and Discussion

Our investigation of the sensitivity of AR identification algorithms associated with changes to the threshold, resolution, and regridding method of the input IVT data set, under one framework, has shown there is considerable uncertainty in detecting global AR occurrence. Coarsening the resolution of the input data leads to a reduced number of ARs, but this result varies depending on the technique used to regrid the data. The bilinear interpolation method produced fewer ARs than conservative regridding or averaging gridboxes. Regridding by averaging led to results from the identification algorithm that were the most similar to the results of using the native IVT field in the algorithm; however, the number of ARs was also sensitive to the order that averaging occurred relative to calculating the IVT. These results may be dependent on the

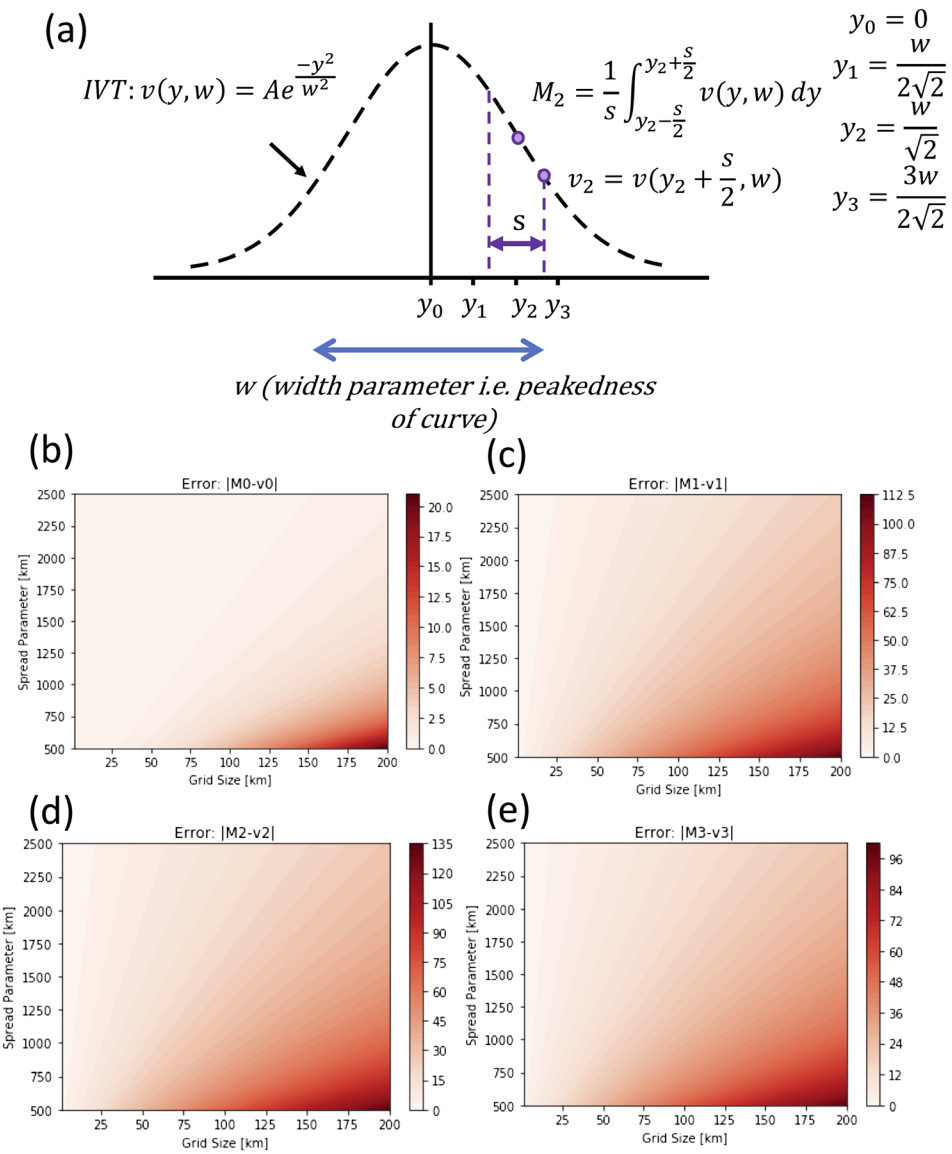

Figure 11. (a) Schematic of idealized AR cross section. s is the length of the grid space (km), w is the width ("peakedness") parameter (km), M is the average IVT over a grid space for different values of s and w (kg m^{-1} s^{-1}), and v is IVT value at the positive edge of the grid space for different values of s and w (kg m^{-1} s^{-1}). (b–e) Maximum error in IVT (kg m^{-1} s^{-1}) for different width parameters and grid spacings at different points along the cross section using our idealized AR cross section.

physical aspects of the specific rivers and the details of the detection algorithm. Nevertheless, we recommend coarsening a grid by averaging or conservative interpolation and caution against using a bilinear interpolation.

Changes to the resolution of the input IVT field affected the number of ARs identified with coarser resolutions resulting in fewer ARs. Hagos et al. (2015) analyzed the resolution dependence of AR frequency in global models. They found a strong resolution dependence using an aquaplanet model (CAM-4), but dependence varied with region in a "real-world" model. Moreover, Swenson et al. (2018) also found in their study of ARs in an aquaplanet that as resolution increased, so did the average monthly frequency of ARs detected. This result has some implications for climate change studies which do not always have the option of using high-resolution IVT fields due to computational costs and model stability requirements. The extent of the implication would depend on the purpose of the study; for example, studies understanding

precipitation changes due to ARs and climate change would be highly vulnerable to resolution-associated uncertainty. Experiments that require detailed analyses of AR counts will have some uncertainty associated with the resolution of the input field; however, studies focusing on the shape and seasonal cycle of the large-scale (global or hemispheric) AR distribution (rather than the magnitude) will likely be less affected by the choice of resolution and regridding method. Nonetheless, the magnitude difference in AR count due to resolution is small especially for grid spaces less than $1.5° \times 1.5°$.

Contrary to other studies (e.g., Guan & Waliser, 2015; Rutz et al., 2014), but similarly to more recent studies (e.g., Rutz et al., 2019), we found high sensitivity in AR algorithm results to the absolute IVT threshold. As expected, and as previous studies also indicated, we found a decrease in AR count as the threshold was increased. However, our experiment shows a spatially heterogeneous change in AR count associated with using different IVT thresholds (Figure 6). The lower 250 kg m^{-1} s^{-1} threshold failed to identify some of the most intense ARs, and in particular intense ARs in the North Pacific and North Atlantic regions, in this study due to unexpected effects of the applied length-to-width ratio criterion. This result disagrees with the conclusion of Rutz et al. (2019) that more restrictive identification methods simply identify a subset of the ARs that the less restrictive methods identify. Figure 9 illustrates that the ARs identified using a higher IVT threshold are not always a subset of those identified with a lower IVT threshold and typically have a greater maximum IVT value. This is concerning given that ARs in these regions are known to cause heavy rainfall and flooding in highly populated locations such as the West Coast of North America and Europe (Lavers et al., 2011; Leung & Qian, 2009; Ralph et al., 2006). From our analysis, we recommend using an IVT threshold of between 350 and 500 kg m^{-1} s^{-1} for global AR studies in the present climate (for absolute threshold methods). Thresholds less than 350 kg m^{-1} s^{-1} risk failing to identify the strongest AR events due to the geometry requirements of some AR algorithms, while IVT thresholds greater than 500 kg m^{-1} s^{-1} will exclude what Ralph et al. (2018) would describe as weak but primarily beneficial ARs. Our results indicate that the commonly used 250 kg m^{-1} s^{-1} IVT threshold is not appropriate for global studies with detection methods that also include a restrictive geometric condition because identification methods with these features can miss some of the strongest storms.

Overall, our results indicate that choice of IVT threshold is the largest source of uncertainty in AR identification algorithms, which is consistent with the literature. Threshold choice affects both the magnitude and location of ARs that are identified. It is important that future identification studies choose a threshold that adequately captures both the high and low extremes of the AR intensity distribution; otherwise, they risk unintentionally excluding the most intense ARs. Finally, the uncertainties within a given AR detection method, including the chosen input data parameters, may be almost as important as uncertainties across AR detection methods.

Data Availability Statement

Atmospheric River Identification Scheme code (MATLAB) produced for this analysis is publicly available and can be accessed from https://figshare.com/articles/software/_/13019096 (https://doi.org/10.26188/13019096). The input data sets used in this study are available from these in-text citation references: Year of Tropical Convection (Waliser et al., 2012) (https://apps.ecmwf.int/datasets/data/yotc-od/levtype=sfc/type=an/) and ERA5 (Hersbach et al., 2019) (https://doi.org/10.24381/cds.adbb2d47). Our submission to ARTMIP using this algorithm can be accessed from (Shields & Kiehl, 2016) (https://www.earthsystemgrid.org/dataset/ucar.cgd.ccsm4.artmip.tier1.html?df=true).

Acknowledgments

The work of K. J. Reid was funded by an Australian Government Research Training Program (RTP) Scholarship and the Australian Research Council (ARC; DE180100638); the work of A. D. King was funded by the ARC (DE180100638); the work of T. P. Lane was funded by the ARC Centre of Excellence for Climate Extremes (CE170100023); and the work of E. Short was funded by the Australian Government RTP Scholarship and ARC Centre of Excellence for Climate Extremes (CE170100023).

References

Brands, S., Gutiérrez, J. M., & San-Martín, D. (2017). Twentieth-century atmospheric river activity along the west coasts of Europe and North America: Algorithm formulation, reanalysis uncertainty and links to atmospheric circulation patterns. *Climate Dynamics*, *48*, 2771–2795. https://doi.org/10.1007/s00382-016-3095-6

Gelaro, R., McCarty, W., Suárez, M. J., Todling, R., Molod, A., Takacs, L., et al. (2017). The Modern-Era Retrospective Analysis for Research and Applications, Version 2 (MERRA-2). *Journal of Climate*, *30*, 5419–5454. https://doi.org/10.1175/JCLI-D-16-0758.1

Gershunov, A., Shulgina, T., Ralph, F. M., Lavers, D. A., & Rutz, J. J. (2017). Assessing the climate-scale variability of atmospheric rivers affecting western North America. *Geophysical Research Letters*, *44*, 7900–7908. https://doi.org/10.1002/2017GL074175

Guan, B., & Waliser, D. E. (2015). Detection of atmospheric rivers: Evaluation and application of an algorithm for global studies. *Journal of Geophysical Research: Atmospheres*, *120*, 12,514–12,535. https://doi.org/10.1002/2015JD024257

Hagos, S., Leung, L. R., Yang, Q., Zhao, C., & Lu, J. (2015). Resolution and dynamical core dependence of atmospheric river frequency in global model simulations. *Journal of Climate*, *28*(7), 2764–2776. https://doi.org/10.1175/JCLI-D-14-00567.1

Hersbach, H., Bell, B., Berrisford, P., Horányi, A., Sabater, J. M., Nicolas, J., et al. (2019). Global reanalysis: Goodbye ERA-Interim, hello ERA5. *ECMWF Newsletter*, *159*, 17–24. https://doi.org/10.21957/vf291hehd7

Hoyer, S., & Hamman, J. J. (2017). Xarray: N-D labeled arrays and datasets in Python. *Journal of Open Research Software*, *5*, 10. https://doi.org/10.5334/jors.148

Lavers, D. A., Allan, R. P., Wood, E. F., Villarini, G., Brayshaw, D. J., & Wade, A. J. (2011). Winter floods in Britain are connected to atmospheric rivers. *Geophysical Research Letters*, *38*, L23803. https://doi.org/10.1029/2011GL049783

Lavers, D. A., Villarini, G., Allan, R. P., Wood, E. F., & Wade, A. J. (2012). The detection of atmospheric rivers in atmospheric reanalyses and their links to British winter floods and the large-scale climatic circulation. *Journal of Geophysical Research*, *117*, D20106. https://doi.org/10.1029/2012JD018027

Leung, L. R., & Qian, Y. (2009). Atmospheric rivers induced heavy precipitation and flooding in the western U.S. simulated by the WRF regional climate model. *Geophysical Research Letters*, *36*, L03820. https://doi.org/10.1029/2008GL036445

Maciel, P., Quintino, T., Modigliani, U., Dando, P., Raoult, B., Deconinck, W., et al. (2017). The new ECMWF interpolation package MIR| ECMWF. Retrieved September 28, 2020, from https://www.ecmwf.int/en/newsletter/152/computing/new-ecmwf-interpolation-package-mir

Neiman, P. J., Ralph, F. M., Wick, G. A., Lundquist, J. D., & Dettinger, M. D. (2008). Meteorological characteristics and overland precipitation impacts of atmospheric rivers affecting the West Coast of North America based on eight years of SSM/I satellite observations. *Journal of Hydrometeorology*, *9*(1), 22–47. https://doi.org/10.1175/2007JHM855.1

Newell, R. E., Newell, N. E., Zhu, Y., & Scott, C. (1992). Tropospheric rivers?—A pilot study. *Geophysical Research Letters*, *19*(24), 2401–2404. https://doi.org/10.1029/92GL02916

Pan, M., & Lu, M. (2019). A novel atmospheric river identification algorithm. *Water Resources Research*, *55*, 6069–6087. https://doi.org/10.1029/2018WR024407

Ralph, F. M., Neiman, P. J., Wick, G. A., Ralph, F. M., Neiman, P. J., & Wick, G. A. (2004). Satellite and CALJET aircraft observations of atmospheric rivers over the eastern North Pacific Ocean during the winter of 1997/98. *Monthly Weather Review*, *132*, 1721–1745. https://doi.org/10.1175/1520-0493(2004)132<1721:SACAOO>2.0.CO;2

Ralph, F. M., Neiman, P. J., Wick, G. A., Gutman, S. I., Dettinger, M. D., Cayan, D. R., & White, A. B. (2006). Flooding on California's Russian River: Role of atmospheric rivers. *Geophysical Research Letters*, *33*, L13801. https://doi.org/10.1029/2006GL026689

Ralph, F. M., Rutz, J. J., Cordeira, J. M., Dettinger, M., Anderson, M., Reynolds, D., & Haase, J. S. (2018). A scale for atmospheric river intensity and potential impacts is introduced, enhancing situational awareness and forecast communication. *Bulletin of the American Meteorological Society*, *100*(2), 269–289. https://doi.org/10.1175/BAMS-D-18-0023.1

Ralph, F. M., Wilson, A. M., Shulgina, T., Kawzenuk, B., Sellars, S., Rutz, J. J., et al. (2019). ARTMIP-early start comparison of atmospheric river detection tools: How many atmospheric rivers hit northern California's Russian River watershed? *Climate Dynamics*, *52*, 4973–4994. https://doi.org/10.1007/s00382-018-4427-5

Rutz, J. J., Shields, C. A., Lora, J. M., Payne, A. E., Guan, B., Ullrich, P., et al. (2019). The Atmospheric River Tracking Method Intercomparison Project (ARTMIP): Quantifying uncertainties in atmospheric river climatology. *Journal of Geophysical Research: Atmospheres*, *124*, 13,777–13,802. https://doi.org/10.1029/2019JD030936

Rutz, J. J., Steenburgh, W. J., & Ralph, F. M. (2014). Climatological characteristics of atmospheric rivers and their inland penetration over the western United States. *Monthly Weather Review*, *142*, 905–921. https://doi.org/10.1175/MWR-D-13-00168.1

Sellars, S., Nguyen, P., Chu, W., Gao, X., Hsu, K., & Sorooshian, S. (2013). Computational earth science: Big data transformed into insight. *Eos, Transactions American Geophysical Union*, *94*, 277–278. https://doi.org/10.1002/2013EO320001

Schulzweida, U. (2019). Climate Data Operators (CDO) User Guide Version 1.9.8, Max Planck Institute for Meteorology. https://doi.org/10.5281/zenodo.2558193

Shields, C. A., & Kiehl, J. T. (2016). Atmospheric river landfall-latitude changes in future climate simulations. *Geophysical Research Letters*, *43*, 8775–8782. https://doi.org/10.1002/2016GL070470

Shields, C. A., Rutz, J. J., Leung, L.-Y., Ralph, F. M., Wehner, M., Kawzenuk, B., et al. (2018). Atmospheric River Tracking Method Intercomparison Project (ARTMIP): Project goals and experimental design. *Geoscientific Model Development*, *11*, 2455–2474. https://doi.org/10.5194/gmd-11-2455-2018

Swenson, E. T., Lu, J., & Straus, D. M. (2018). Resolution dependence and Rossby wave modulation of atmospheric rivers in an Aquaplanet model. *Journal of Geophysical Research: Atmospheres*, *123*, 6297–6311. https://doi.org/10.1029/2017JD027899

Trenberth, K. E., Dai, A., Rasmussen, R. M., & Parsons, D. B. (2003, September). The changing character of precipitation. *Bulletin of the American Meteorological Society*, *84*, 1205–1218. https://doi.org/10.1175/BAMS-84-9-1205

Viale, M., Valenzuela, R., Garreaud, R. D., & Ralph, F. M. (2018). Impacts of atmospheric rivers on precipitation in southern South America. *Journal of Hydrometeorology*, *19*, 1671–1687. https://doi.org/10.1175/JHM-D-18-0006.1

Waliser, D. E., Moncrieff, M. W., Burridge, D., Fink, A. H., Gochis, D., Goswami, B. N., et al. (2012). The "year" of tropical convection (May 2008–April 2010): Climate variability and weather highlights. *Bulletin of the American Meteorological Society*, *93*(8), 1189–1218. https://doi.org/10.1175/2011BAMS3095.1

Wick, G. A., Neiman, P. J., & Ralph, F. M. (2013). Description and validation of an automated objective technique for identification and characterization of the integrated water vapor signature of atmospheric rivers. *IEEE Transactions on Geoscience and Remote Sensing*, *51*, 2166–2176. https://doi.org/10.1109/TGRS.2012.2211024

Zhu, Y., Newell, R. E., Zhu, Y., & Newell, R. E. (1998). A proposed algorithm for moisture fluxes from atmospheric rivers. *Monthly Weather Review*, *126*(3), 725–735. https://doi.org/10.1175/1520-0493(1998)126<0725:APAFMF>2.0.CO;2